



Large-scale brain mediation network based on resting-state functional MRI

Received: 20 May 2025

Bin Wang ¹, Xi Zhang ¹, Tingting Pan ¹, Ting Li ², Tiantian Liu ³ & Tianyi Yan ³

Accepted: 24 September 2025

Published online: 17 November 2025

Check for updates

Exploring the brain's complex interaction mechanisms is vital for understanding its functions. Traditional network models typically simplify brain region interactions into pairwise connections. However, such interactions may be significantly modulated by a third brain region. Given the widespread connections among numerous regions at the whole-brain scale, constructing an accurate model of brain triple-region interactions is challenging. Here, we develop an independent component-driven mediation brain network model that captures triple-region mediation relationships while controlling extraneous influences. Our results reveal an inverted U-shaped relationship between mediated strength and degree strength, indicating distinct mediation patterns in dense and sparse connected regions. Furthermore, the primary sensory and attention modules exhibit functional hierarchical differentiation: areas responsible for primary information processing belong to the super mediation set, while regions involved in higher-order cognitive functions belong to the super mediated set. These results emphasize the distinct influences of different mediation patterns on the cognitive capabilities of the brain.

The brain is not merely a collection of isolated structures, but rather operates as a complex and highly interconnected network system. Within this system, specialized brain regions dynamically interact and collaborate to execute complex cognitive, emotional, and sensorimotor tasks¹. For example, the visual cortex works in concert with the temporal lobe to interpret visual information², whereas the motor cortex coordinates with the cerebellum to control precise movements³. Furthermore, the brain undergoes a gradual change from localized regions to distributed modules during development, ultimately enhancing its capacity for collaboration among diverse modules⁴. This intricate network organization underscores the brain's ability to integrate information across specialized regions or modules, enabling efficient and adaptive functioning⁵. Consequently, understanding the brain as an interconnected network system is critical in unraveling the neural basis of human functions.

With the advancement of modern neuroimaging techniques, resting-state functional magnetic resonance imaging (fMRI) offers a

comprehensive and non-invasive means to explore the organization of the human brain's functional network. It enables the measurement of neural activity interaction between remote brain regions using blood oxygen level-dependent (BOLD) signals⁶, thereby allowing for the examination of functional connectivity (FC) on a whole-brain scale. Utilizing diverse statistical dependencies, including correlation⁷, coherence⁸, and Granger causality⁹, of the BOLD time series, a large number of researchers have computed the pairwise interactions between brain regions. However, it has been revealed that the brain exhibits not only binary interactions but also extensive interactions among multiple brain regions^{10,11}. For example, the parahippocampal gyrus acts as a bridge connecting the hippocampus and the posterior cingulate cortex¹², while FC within the thalamus-amygdala pathway is modulated by the prefrontal lobe during fear perception¹³. These studies emphasize that the information transfer between two brain regions may involve the participation or influence of a third brain region¹⁴. Therefore, shifting our focus from pairwise to multivariate

¹College of Computer Science and Technology (College of Data Science), Taiyuan University of Technology, Taiyuan, China. ²School of Software, Taiyuan University of Technology, Taiyuan, China. ³School of Medical Technology, Beijing Institute of Technology, Beijing, China. e-mail: tiantian2bit@bit.edu.cn; yantianyi@bit.edu.cn

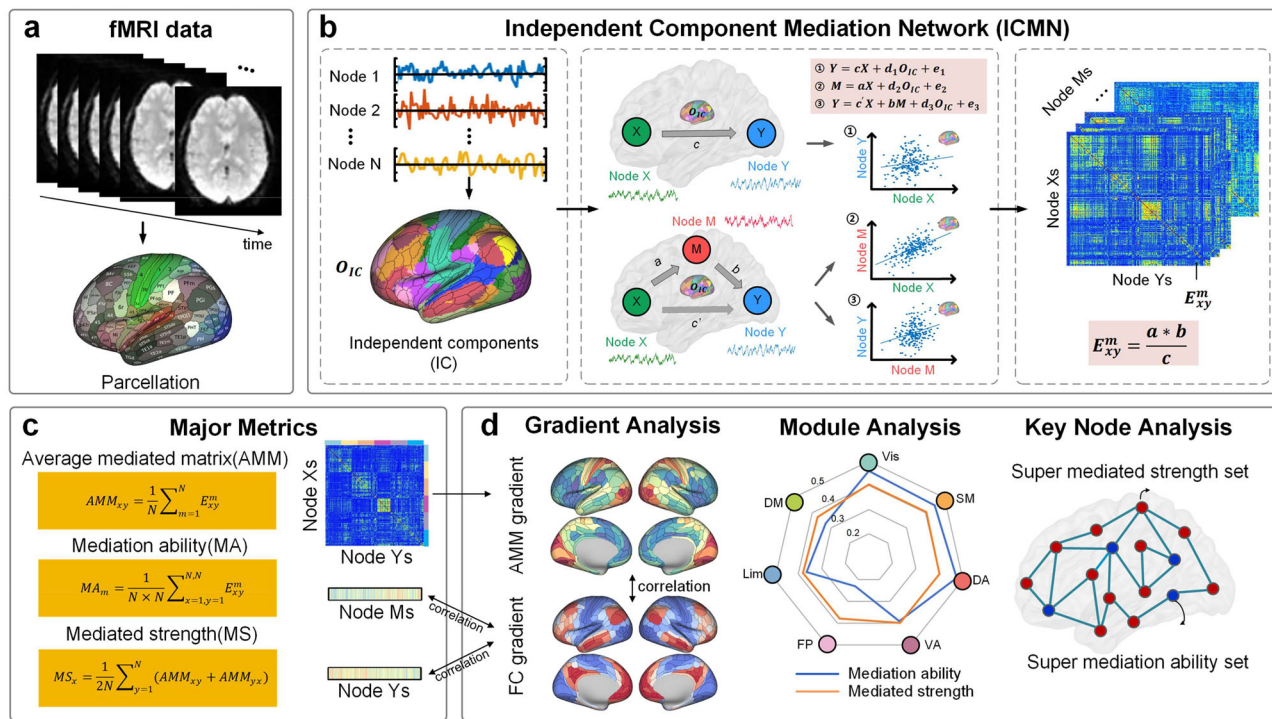


Fig. 1 | Schematic diagram for the construction of the brain independent component mediation network (ICMN). **a** The fMRI brain data, which was parcellated into BOLD signals of N regions. **b** The fundamental principle guiding the construction of the brain ICMN. **c** The formula employed for computing average mediated matrix (AMM), MA, and MS. **d** A comprehensive analysis of these metrics, including gradient analysis, module analysis, and key node analysis. The gradient

analysis evaluated the gradient of AMM and the functional connectivity (FC) matrix. Furthermore, correlations between MA/MS and the gradient of the FC matrix are calculated. The module analysis assessed the average value of the metrics for the nodes within each module. The key node analysis identified the super mediation ability set (super-MAs, highlighted in blue) and the super mediated set node (super-MSs, highlighted in red).

interactions can provide deeper insights into the complex dynamics of brain networks.

Various methodologies have been utilized to analyze multivariate relationships, with mediation analysis emerging as a particularly effective tool^{15–18}. This technique is indispensable for investigating the impact of one variable on an outcome, which is partially or fully mediated by another variable¹⁹. Numerous studies have investigated mediation analysis to assess multivariate relationships in brain networks^{20–22}. For example, Kim et al. explored the information flow patterns within the triple network by utilizing the mean BOLD signals from the default-mode, central executive, and salience networks in mindfulness²³. Chen et al. extended mediation analysis to high-dimensional levels, treating the entire brain network as a single composite mediator variable to explore the neural characteristics mediating behavioral symptoms and psychotic episodes²⁴. Nevertheless, the above studies are limited to analyzing interactions in small-scale scenarios involving only three variables. Indeed, the human brain possesses an extremely complex structure, typically comprising hundreds of distinct regions^{25,26}. There exists a lack of network models that measure mediation relationships among large-scale regions. Moreover, the brain regions exchange and transmit information with a large number of others to varying degrees^{27,28}. It is not feasible to simply assume that the interactions between the currently analyzed three brain regions are completely independent of the influence exerted by other brain regions within the network model²⁹. Thus, developing a network model that can capture the multifaceted relationships among brain regions and effectively remove potential interference from other brain regions remains a significant challenge.

In this study, we design an ICMN model to characterize multiple interactions of resting-state brain fMRI data. The model explores how the interaction between any two brain regions is modulated by another region, while eliminating the influence of the remaining regions across

the whole brain. To further characterize individual brain mediation network differences, we introduce several mediation parameters, including the mediation ability (MA) and mediated strength (MS). Finally, the underlying mechanisms of brain mediation networks are explored by gradient and cognitive correlation analysis. Our findings will contribute to a deeper understanding of triple-wise interactions among brain regions and the higher-order organization of intrinsic human brain networks.

Results

We constructed whole-brain ICMN from fMRI data through three key steps (Fig. 1a–c). First, we extracted time series from N brain regions using a standard template²⁵ (Fig. 1a). The resulting $N \times N \times N$ matrix quantified mediation effects (M 's influence on X – Y connection) as the ratio of indirect ($a \times b$) to total effects (c), where a and b represent $X \rightarrow M$ and $M \rightarrow Y$ path coefficients, respectively. To control for remaining regions' influences, we applied independent component analysis (ICA) to reduce regional time series to 20 components for mediation calculations in simulated data and real data from Human Connectome Project (HCP) dataset (Fig. 1b). For the selection of 20 components, we conducted a systematic quantitative assessment of the range from 5 to 70 components (with a step size of 5) by analyzing the contribution rate of independent components to the reconstruction of the original signal. We found that when the number exceeded 20, the growth rate of the contribution rate slowed significantly. The specific calculation methods and results are detailed in the Supplementary Methods and Supplementary Fig. 1. Additionally, the results for 10 and 30 components are also presented in the Supplementary Figs. 2–15. The validation results for the Chinese Human Connectome Project (CHCP) dataset are presented in the Supplementary Figs. 16–18.

Based on the $N \times N \times N$ -connected mediation network, we further calculated three metrics, including average mediated matrix (AMM),

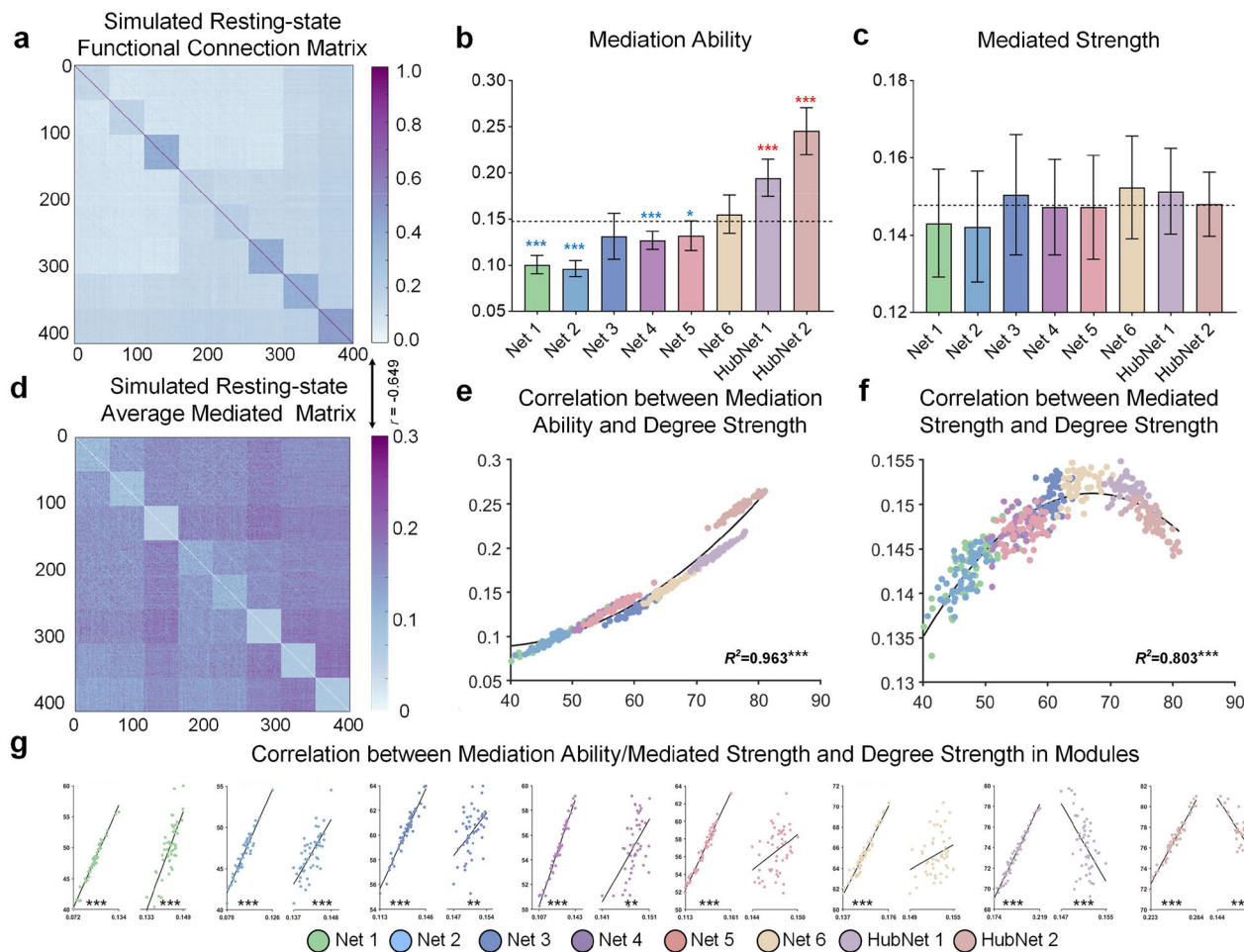


Fig. 2 | Results of ICMN modeling in simulated data. The simulated (a) FC and (d) AMM of 400 brain regions, including 2 hub networks and 6 non-hub networks. The color bars represent the value of FC and AMM, respectively, with darker colors indicating greater intensity. The (b) MA and (c) MS of each brain module. The error bars in box plots represent the standard deviation. The black dashed line represents the mean values of MA/MS for all modules. Red * represents significantly

higher than the mean, and blue * represents significantly lower. The sample size of virtual subjects is 30. (e, f) The correlations between MA/MS with FC degree strength at the whole-brain level. (g) The correlations of MA/MS with FC degree strength at the module level. Different colors in the diagram correspond to different modules. The correlation analysis is based on data from 400 brain regions averaged from the subjects. * $p < 0.05$, ** $p < 0.01$, and *** $p < 0.001$.

MA, and MS (Fig. 1c). In the connection level, AMM reflects the average degree of mediation in communication between node pairs by all other mediator nodes. At the regional level, MA quantifies a node's average capacity to facilitate communication as a mediator. MS measures a node's average strength of mediation when it communicates with other nodes through mediator nodes. Subsequently, we conducted further analyses of these metrics, including gradient analysis, module analysis, and key node of super mediation ability set (super-MAs) and super mediated strength set (super-MSs) analysis (Fig. 1d).

Simulation study results

To verify the performance of ICMN in capturing the mediation patterns in modules with different connection strengths, we created a simulated brain network structure with 400 regions organized into 8 network communities (2 hub and 6 non-hub modules), and generated simulated BOLD time series. Based on these time series, we constructed ICMN and computed mediation metrics, including the AMM, MA, and MS. Additionally, the simulated FC matrix was estimated to compare the ICMN with traditional functional connectivity patterns (Fig. 2a). At the connection level, we found a significant negative correlation between AMM and FC matrix (Spearman correlation, $r = -0.649$, $p < 0.001$) (Fig. 2d), indicating less mediation in tightly

functionally connected regions. In the regional level, we found the MA and MS distributions varied across modules, particularly the hub module exhibited higher MA (Fig. 2b, c). Furthermore, we investigated the correlations between MA/MS and FC topology metrics. As shown in Fig. 2e, f, the degree strength showed positive correlations with MA ($R^2 = 0.963$, $p < 0.001$), while showing inverted U-shaped correlations with MS ($R^2 = 0.803$, $p < 0.001$). At the module level, the MA of each module showed a significant positive correlation with degree strength. The MS and degree strength of two hub modules were significantly negatively correlated, while four non-hub modules were significantly positively correlated (Fig. 2g). Detailed statistical values are presented in the Supplementary Tables 1 and 2.

Brain mediation network metrics at the whole-brain level

Based on the exploration of mediation patterns in simulated time series, we further applied ICMN to real BOLD time series. We found that AMM was highly negatively correlated with FC matrix (Spearman correlation, $r = -0.478$, $p < 0.001$) (Fig. 3a, b). The results of the MA showed strong values in the primary visual, somatosensory, and motor cortex (Fig. 3c). In addition, the results of the MS showed strong values in the secondary visual, secondary motor, insular, and cingulate cortex (Fig. 3d).

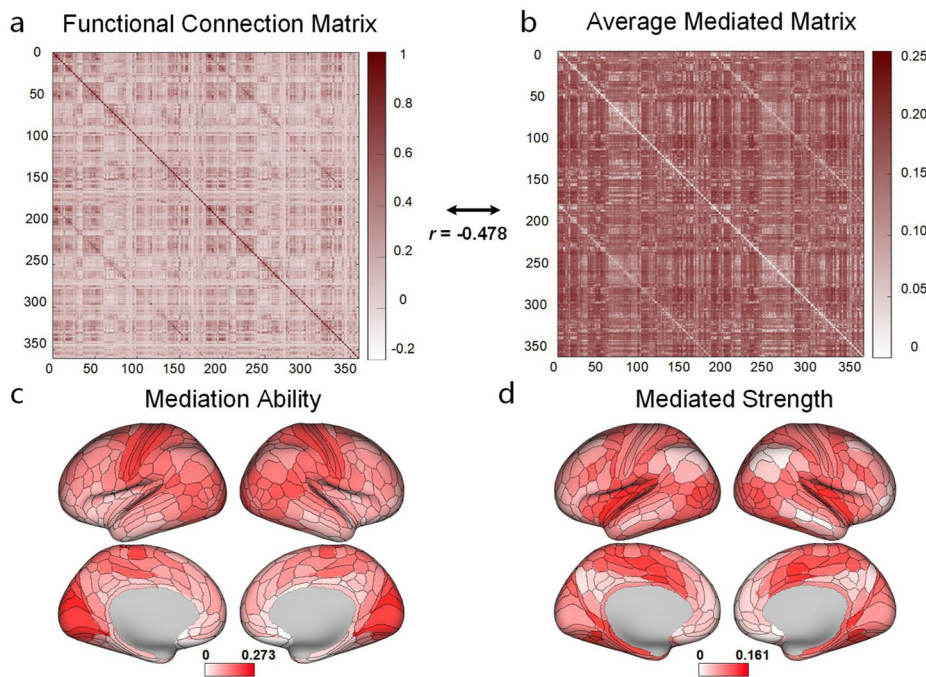


Fig. 3 | The brain mediation network metrics at the whole-brain level. The whole-brain **a** resting-state FC matrix and **b** AMM. The spatial distribution map of **c** MA and **d** MS. The color bars represent the value of mediation network metrics, with darker colors indicating greater intensity.

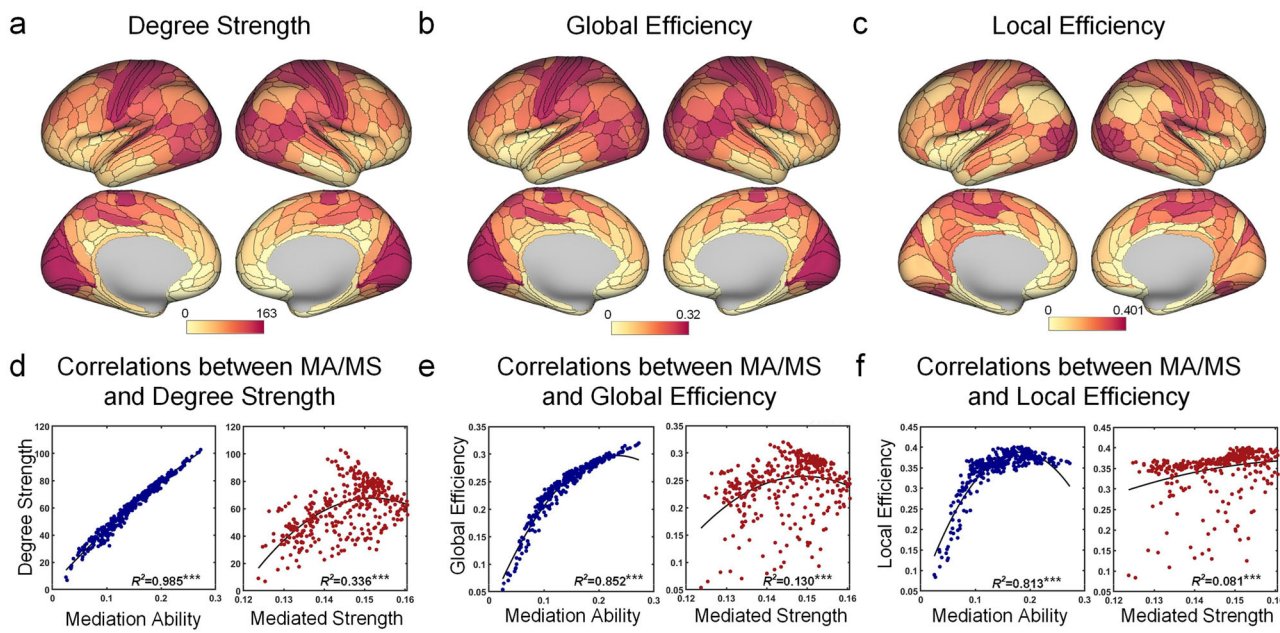


Fig. 4 | The FC topological metrics and their correlations with MA/MS at the whole-brain level. The spatial distribution map of **a** degree strength, **b** global efficiency, and **c** local efficiency. The color bars represent the value of FC topological metrics, with darker colors indicating greater intensity. Correlations between

MA/MS and FC topological properties, including **d** degree strength, **e** global efficiency, and **f** local efficiency. The correlation analysis is based on data from 360 brain regions averaged from the subjects. * $p < 0.05$, ** $p < 0.01$, and *** $p < 0.001$.

Correlations between MA/MS and FC topological metrics at the whole-brain level

We also assessed the correlations between MA/MS and FC topological metrics, including nodal degree strength (Fig. 4a), global efficiency (Fig. 4b), and local efficiency (Fig. 4c). The AIC assessment revealed quadratic correlations between these variables (Fig. 4d-f). In particular, both degree strength ($R^2 = 0.986$, $p < 0.001$) and global efficiency ($R^2 = 0.951$, $p < 0.001$) showed positive correlations with MA, while local efficiency exhibited an inverted U-shaped pattern

($R^2 = 0.813$, $p < 0.001$) with MA. Conversely, both degree strength ($R^2 = 0.336$, $p < 0.001$) and global efficiency ($R^2 = 0.130$, $p < 0.001$) showed inverted U-shaped correlations with MS, while local efficiency demonstrated a positive correlation with MS ($R^2 = 0.083$, $p < 0.001$).

Correlations between functional gradients and mediation network metrics at the whole-brain level

In order to analyze the functional organization pattern of brain networks, we computed the primary gradient of the group-averaged FC

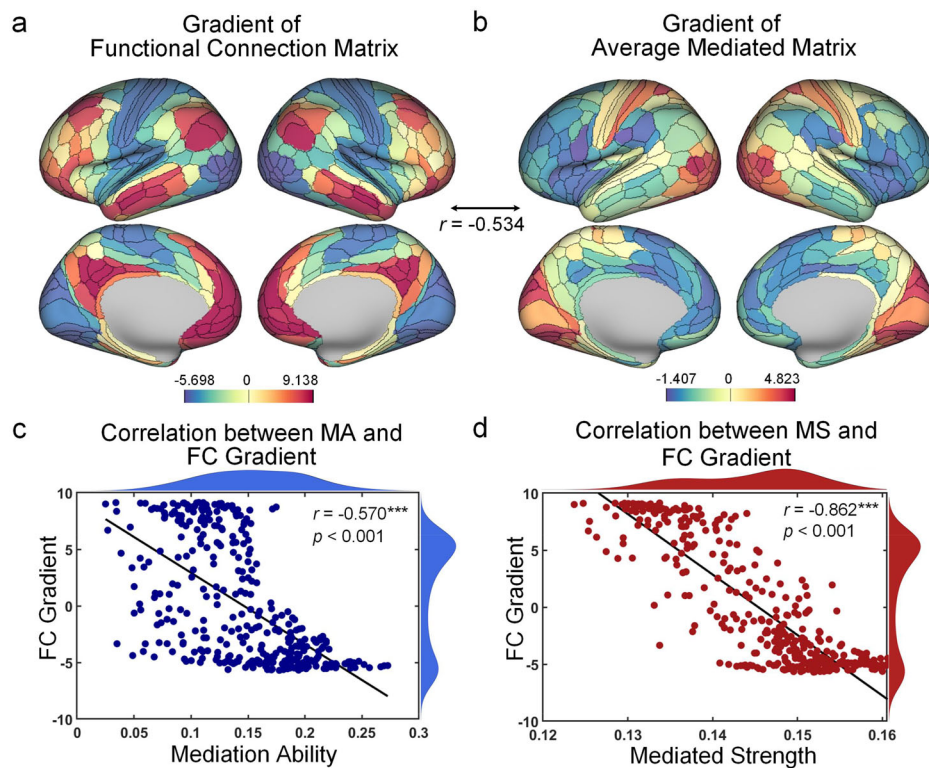


Fig. 5 | Correlations between functional gradients and mediation network metrics at the whole-brain level. The primary gradient of the **a** group-averaged FC matrix and **b** AMM. The color bars represent gradient values from negative (blue) to positive (red), with white corresponding to zero. **c, d** The correlations between MA/

MS with the primary gradient of the FC matrix, respectively. The correlation analysis is based on data from 360 brain regions averaged from the subjects. $p < 0.05$, $p < 0.01$, and $^{***}p < 0.001$.

matrix (Fig. 5a) and AMM, respectively. Furthermore, we investigated the relationship between them and found that they were significantly negatively correlated (Spearman correlation, $r = -0.534$, $p < 0.001$) (Fig. 5b). Additionally, both the MA (Spearman correlation, $r = -0.570$, $p < 0.001$) (Fig. 5c) and MS (Spearman correlation, $r = -0.862$, $p < 0.001$) (Fig. 5d) demonstrated significant negative correlations with FC gradient.

Brain mediation network metrics at the module level

We then map the mediation metrics to seven functional modules, including visual (Vis), somatomotor (SM), dorsal attention (DA), ventral attention (VA), frontoparietal (FP), limbic (Lim), and default mode (DM) modules. FC matrix and AMM of these seven functional modules were calculated (Fig. 6a, b). In the module analysis of MA and MS, we found that Vis, SM and DA exhibited significantly higher MA than the average value, while FP, Lim, and DM exhibited significantly lower MA than the average value (Fig. 6c). However, no significant differences were found between module MS and the average value (Fig. 6d). Detailed statistical values are presented in the Supplementary Table 3.

Correlations between MA/MS and FC topological metrics at the module level

The degree strength, global efficiency, and local efficiency of seven modules are shown in Fig. 7a-c. We found that the MA exhibited significant positive correlations with both degree strength and global efficiency in all modules. The MS exhibited significant negative correlations with both degree and global efficiency in Vis and SM modules, and significant positive correlations with degree strength in Lim and DM modules (Fig. 7d, e). For local efficiency, the MA exhibited an inverted U-shaped relationship with local efficiency in most modules, except for the Lim module, where they were positively correlated. Additionally, the MS was positively correlated with local efficiency in

the Vis, SM, and DA modules (Fig. 7f). Detailed statistical values are presented in the Supplementary Tables 4-7.

Correlations between functional gradients and mediation network metrics at the module level

We then map the gradient of FC and AMM to seven functional modules (Fig. 8a, b). We found significant negative correlations between the FC and AMM gradient scores in the Vis, SM, DA, and DM modules. Additionally, a significant negative correlation was found between the MA of the DA module and FC gradient, and significant negative correlations were found between the FC gradient and MS in the DA, VA, FP, Lim, and DM modules (Fig. 8c). Detailed statistical values are presented in Supplementary Tables 8 and 9.

The distribution of super-MAs and super-MSs

Using k-means clustering, we categorized MA and MS into three clusters, respectively, identifying super-MAs and super-MSs with the highest values. We found the super-MAs were mainly located in the primary visual cortex of Vis, the central anterior and posterior gyrus of SM, and the inferior parietal lobular portion of VA. Additionally, the superior parietal lobule and temporo-parieto-occipital junction cortex belonging to the DA were also identified as super-MAs (Fig. 9a). The super-MSs were located mainly in the secondary visual area of Vis, posterior insular cortex, and paracentral lobule of SM, posterior inferotemporal gyrus of DA, as well as the part of VA including anterior insular cortex and mid cingulate gyrus. The hippocampal parahippocampal gyrus, which is part of the Lim module, was also classified as the super-MSs (Fig. 9b). Then, the correlations between the values of super-MAs/super-MSs and cognitive functions were established. Significant correlations found: super-MAs values with self-regulation (Spearman correlation, $r = 0.175$, $p = 0.018$) (Fig. 9c), and super-MSs values with episodic memory (Spearman correlation, $r = 0.152$,

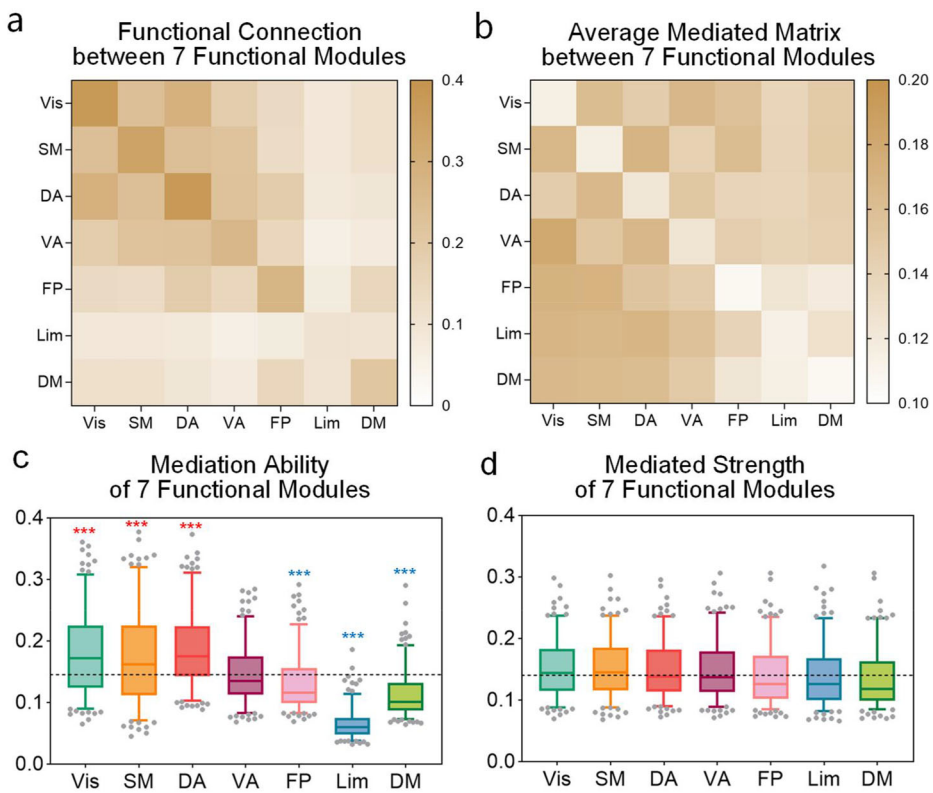


Fig. 6 | The brain mediation network metrics at the module level. The **a** FC matrix and **b** AMM in seven functional modules. The color bars represent the value of FC and AMM, respectively, with darker colors indicating greater intensity. The **c** MA and **d** MS of seven functional modules. The black line in the violin diagram

represents the mean values of MA/MS for all modules. The error bars in box plots represent the standard deviation. Red * represents significantly higher than the mean, and blue * represents significantly lower. The sample size of subjects is 200. * $p < 0.05$, ** $p < 0.01$, and *** $p < 0.001$.

$p = 0.040$) (Fig. 9d). The results regarding the associations between super-MAs/super-MSs and additional cognitive tasks are available in the Supplementary Tables 10 and 11.

Cognition prediction capability by super-MAs and super-MSs values

We utilized an advanced connectome-based predictive modeling (CPM) approach to assess the predictive capability of super-MAs and super-MSs values for cognitive functions, respectively. Model performance was evaluated using Spearman correlation on predicted and actual behavior scores. As shown in Table 1, the prediction model based on super-MAs and super-MSs values can well predict cognitive scales.

Discussion

We developed a network model, named the brain independent component mediation network (ICMN), to quantify the multivariate relationships of large-scale fMRI time series data. This mediation network is capable of measuring the information transmission among any three regions, while eliminating the influence of other brain regions. These preliminary discoveries emphasize the significance of multivariate interactions within brain networks and further propel our understanding of human brain functions.

Applying ICMN to both simulated and real fMRI data, we quantified mediation network metrics, including AMM at the connection level and MA/MS at the regional level, followed by an investigation of their associations with conventional FC measures. Specifically, AMM reflected the average mediated influence between regions, showing weaker within-module than between-module mediation and a negative correlation with the FC matrix. This suggests that strongly connected regions rely less on indirect mediation for information transfer³⁰. MA

represented a region's capacity to facilitate communication as a mediator, was higher in hub modules and positively correlated with degree strength at both whole-brain and module levels, reinforcing their role in network-wide integration³¹. Conversely, MS, which captures a region's dependence on mediated pathways, exhibited an inverted U-shaped relationship with degree strength at the whole-brain level. In the further module-level analyses, we observed densely connected hub modules of simulated data (Vis and SM of real fMRI data) displayed a negative correlation with degree strength, which was consistent with the negative correlation between AMM and FC matrix in dense connected hub modules. However, sparsely connected non-hubs modules of simulated data (Lim and DM of real fMRI data) trended toward increased MS with higher degree strength, suggesting greater reliance on indirect mediation when direct connections are insufficient. We speculate that, in the sparsely connected module, when the direct connection between two regions is not strong enough to maintain the normal communication requirements, the information transfer mediated by other regions may be performed more often³². Therefore, increased MS offers numerous opportunities for communication, thereby increasing the degree strength³³.

These findings were further supported by real brain network efficiency analyses. MA correlated positively with global efficiency at both whole-brain and module levels. Global efficiency is calculated as the inverse average of the shortest path lengths in the network. High global efficiency means that information can be transmitted efficiently through shorter paths in the network^{34,35}. This suggests that regions with high MA possess robust information processing capabilities, pivotal for brain-wide information integration. While MS exhibited an inverted U-shaped association with global efficiency, with dense modules (including Vis and SM) showing reduced efficiency at high MS and sparse modules (including Lim and DM) increased efficiency at

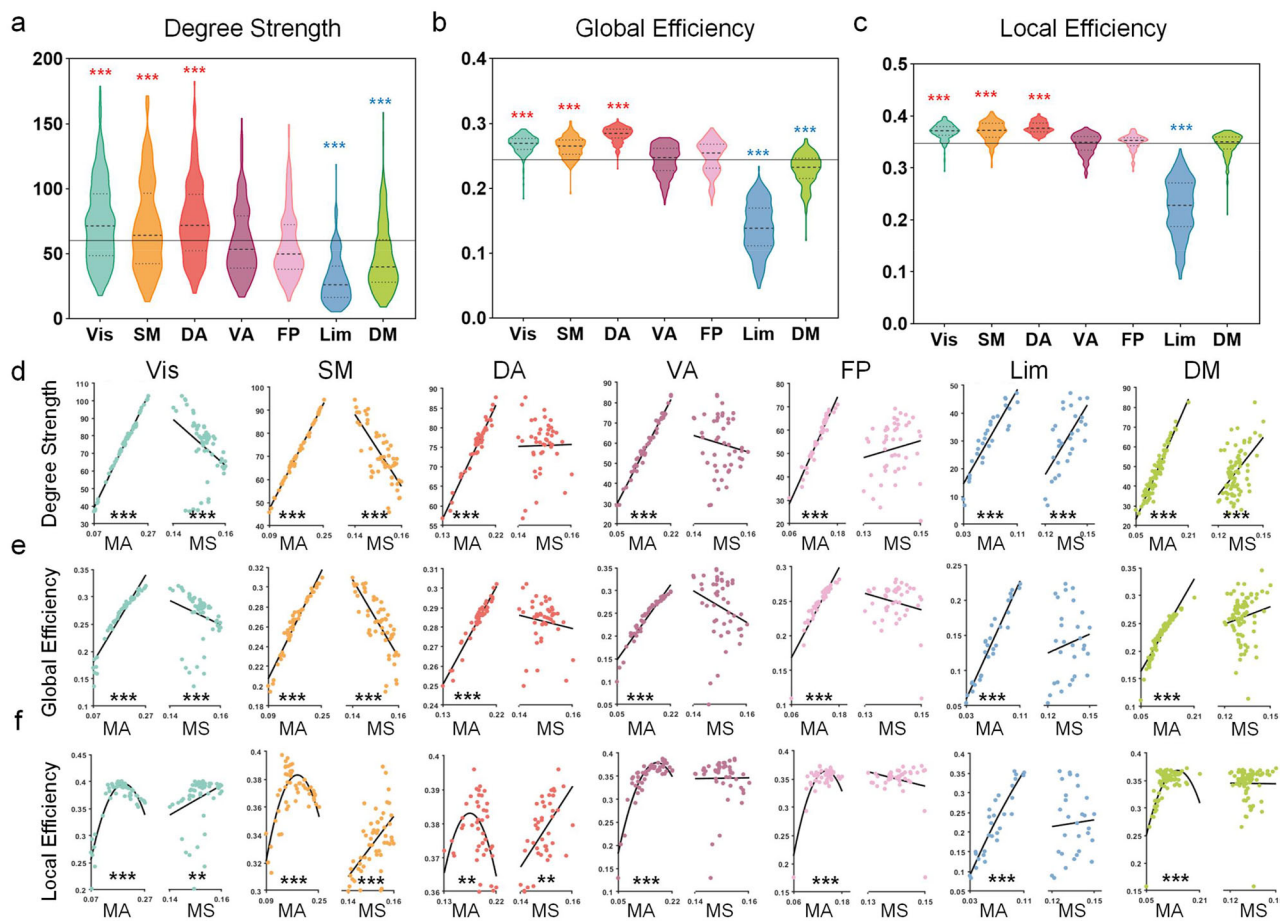


Fig. 7 | The FC topological metrics and their correlations with MA/MS at the module level. The FC topological properties, including a degree strength, b global efficiency, and c local efficiency of seven functional modules. The black line in the violin diagram represents the mean values of FC topological metrics for all modules. Red * represents significantly higher than the mean, and blue * represents

significantly lower. The sample size of subjects is 200. d-f The relationship between MA/MS and FC topological properties of seven functional modules, respectively. The correlation analysis is based on data from distinct functional modules averaged from the subjects. $p < 0.05$, $^*p < 0.01$, and $^{***}p < 0.001$.

high MS. In densely connected modules, nodes preferentially form direct connections, resulting in lower MS values, shorter path lengths, and faster transmission efficiency³⁶. In contrast, sparsely connected modules exhibited longer path lengths, suggesting mediated pathways may partially compensate for weaker direct connectivity by facilitating alternative information routes. Furthermore, we observed an inverted U-shaped correlation between MA and local efficiency, indicating that local efficiency peaks at an optimal MA level. Local efficiency reflects the brain's capacity for localized information processing and resilience to small-scale disruptions^{34,35}. When MA exceeds a threshold, excessive coordination may lead to information overload, reducing the brain's resilience. Additionally, MS and local efficiency showed a positive correlation. This implies that more indirect connectivity pathways mediated by other nodes may facilitate decentralized storage and processing of information^{10,37}. This enhances the brain's fault-tolerance and adaptability, resulting in higher local efficiency.

To investigate the patterns of brain organization reflected by the mediation network, we utilized the diffusion mapping to explore the gradient of AMM. Gradients help reduce dimensionality of brain connectivity data and capture continuous changes in brain spatial distribution structure^{38,39}. Prior FC gradients showed direct connectivity strength changes, revealing specific functional separations formed by the spatial structural arrangement of different brain regions^{40,41}. The AMM measures the degree to which communication between two brain regions is mediated by other nodes, reflecting to some extent the indirect connectivity strength between these two brain regions. Thus,

we calculated the AMM gradient to reflect continuous changes in indirect pathway connectivity. The principal gradient of AMM decreases from unimodal sensorimotor to transmodal association areas, aligning with the FC gradient. This suggests the topography of indirect connections is also not randomly distributed, but rather spatially organized along the gradient axis from unimodal to transmodal areas. Compared with the primary sensory modules, higher-order cognitive modules exhibit the most different patterns of indirect connectivity⁴². These findings provide complementary insights into the hierarchical organization of brain networks beyond direct connectivity measures.

To reveal the mediation network patterns of different modules, we computed the MA and MS of each module separately. The results showed that higher MA was found in the Vis, SM, and DA modules. MA represents the strength of a node's role in controlling the connectivity pathways within a brain network. A higher MA in a brain region means stronger connections to other regions. The result validated the conclusion that the primary sensory modules exhibit more direct and short-range connections^{37,43-45}. In contrast, the FP, Lim, and DM modules show limited MA. The connections of these higher-order cognitive modules to other brain regions are relatively sparse or indirect, allowing the brain to integrate information in a more flexible manner^{37,43-45}. For example, upon receiving preliminary sensory stimuli, the DA module selectively adjusts the intensity and direction of attention^{46,47}. This feedback can directly act on primary perception modules to rapidly optimize the capture and processing of critical

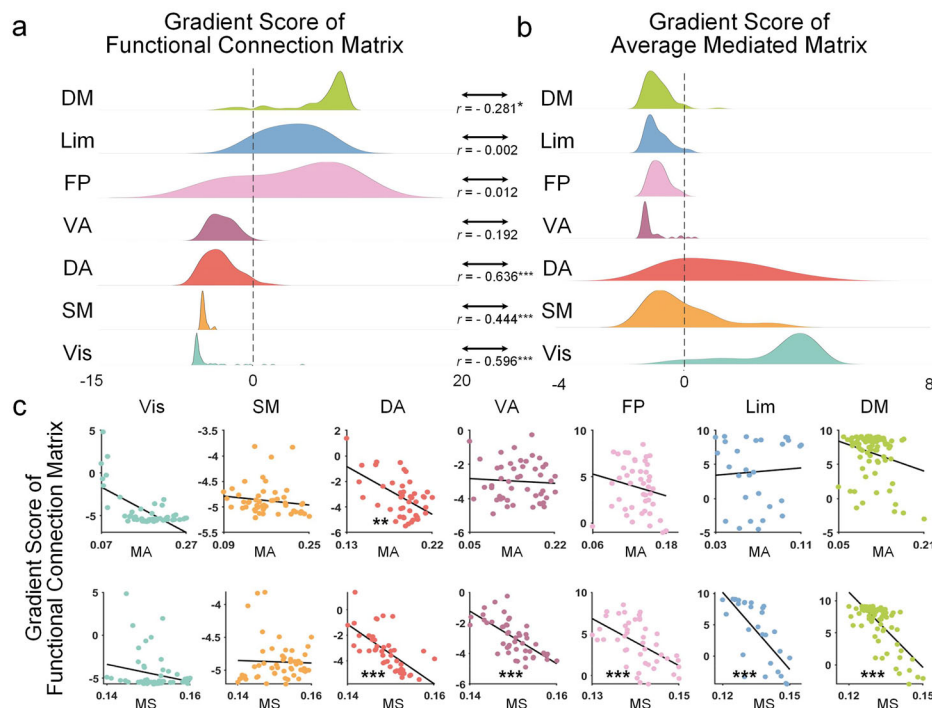


Fig. 8 | Correlations between functional gradients and mediation network metrics at the module level. The primary gradient scores of the **a** FC matrix **b** AMM of seven functional modules. **c** The relationship between MA/MS with the

primary gradient of the FC matrix of seven functional modules. The correlation analysis is based on data from distinct functional modules averaged from the subjects. $p < 0.05$, $**p < 0.01$, and $***p < 0.001$.

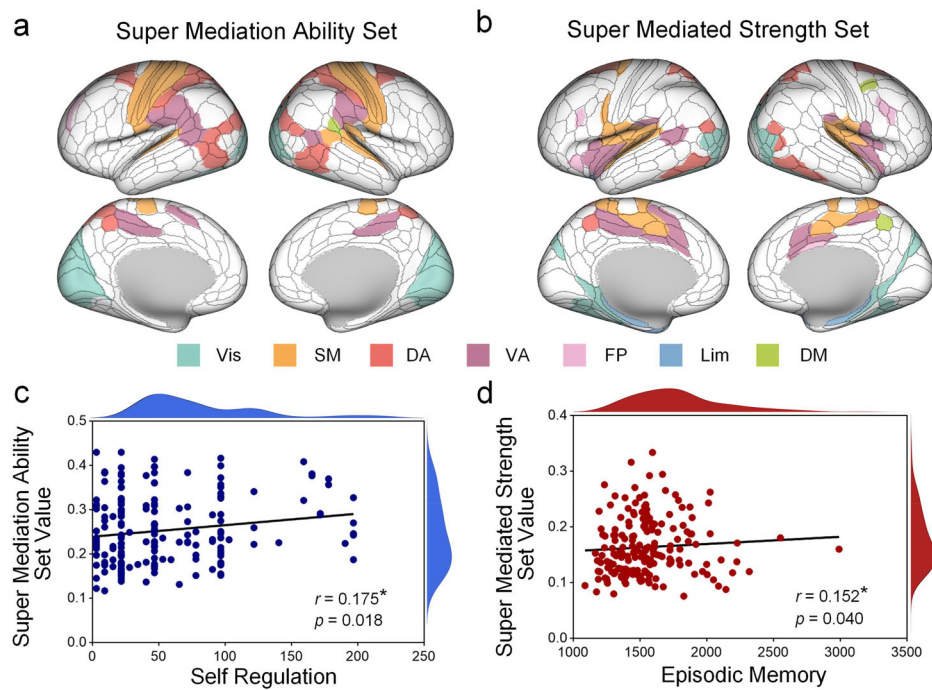


Fig. 9 | The super-MAs/super-MSs and their correlations with cognitive ability. The spatial distribution map of **a** super-MAs and **b** super-MSs. The cognitive ability related to **c** super-MAs value and **d** super-MSs value is significant. The sample size of subjects is 200. $p < 0.05$.

information⁴⁸ or involve advanced cognitive modules to complete more complex responses or decision-making processes⁴⁹. This mechanism significantly enhances the efficiency of the interaction between the primary sensory module and the DA module⁵⁰, both of which play an indispensable mediation role in the information processing process. However, the mediation role played by higher-order

cognitive modules in transmitting sensory information to higher-level cognitive processing stages is more indirect and complex⁵¹.

We further identified brain regions with the highest MA/MS values as super-MAs/super-MSs to examine their roles in information processing. Notably, the Vis, SM, DA, and VA modules exhibited the existence of both super-MAs and super-MSs, in which the distribution

Table 1 | Prediction results from super-MAs and super-MSs values

		Super-MAs	Super-MSs
Self regulation	<i>r</i>	0.316	0.358
	<i>p</i>	<0.001	<0.001
Episodic memory	<i>r</i>	0.160	0.233
	<i>p</i>	<0.001	<0.001
Vocabulary comprehension	<i>r</i>	0.303	0.298
	<i>p</i>	<0.001	<0.001
Emotion regulation	<i>r</i>	0.193	0.396
	<i>p</i>	0.009	<0.001
Fluid intelligence	<i>r</i>	0.285	0.474
	<i>p</i>	<0.001	<0.001
Crystallized cognition	<i>r</i>	0.441	0.279
	<i>p</i>	<0.001	<0.001

Bold values indicate significant correlations between predicted and actual scores on the cognitive scale, with statistical significance set at $p<0.001$.

of super-MAs is very similar to the hub nodes in FC networks^{31,44,52}. We speculate that the existence of both super-MAs and super-MSs within a module reflects the collaboration and balance of brain function in hierarchical information processing. For instance, in the Vis module, the super-MAs are primarily distributed in the primary visual cortex. As a hub node, it exhibits extensive connections both within and outside the module, responsible for the rapid and efficient transmission and integration of visual information^{53,54}. In contrast, the super-MS is located in the secondary visual cortex. These regions may engage in higher-order visual processing, such as shape recognition, through interactions mediated by the primary cortex, contributing to balanced information transmission⁵⁵⁻⁵⁷. Similarly, in the SM module, the motor and somatosensory cortices serve as super-MAs, directly participating in motor command output and sensory feedback⁵⁸. Meanwhile, the posterior insular cortex and paracentral lobule function as super-MSs, achieving complex motor sequence planning and fine tactile information processing through interactions mediated by the primary cortex⁵⁹. The DA and VA modules also exhibit similar differentiation: the super-MAs (including parietal cortex, temporo-parieto-occipital junction) are responsible for spatial attention orientation and visual guidance^{46,60}. The super-MSs (including fusiform gyrus, anterior insular cortex, and mid-cingulate cortex) may accomplish spatial relationship representation and emotional stimulus attention regulation through interactions with mediator nodes^{61,62}. In contrast, advanced cognitive modules (including FP, Lim, DM), which rely on distributed, non-hierarchical information integration, show weaker differentiation between mediation and mediated roles among their nodes, reflecting the complex nature of advanced cognitive functions⁴⁵.

Our analysis revealed significant relationships between brain mediation patterns and cognitive functions, with super-MA values showing positive correlation with self-regulation and super-MS values correlating with episodic memory performance. The self-regulation association primarily involves perceptual and attentional regions, where perceptual areas provide essential external information input⁶³ while attentional modules guide focus and behavioral adjustment⁶⁴, working synergistically to maintain adaptive responses to environmental demands⁶⁵. For episodic memory, the super-MS related regions included the hippocampus for memory consolidation⁶⁶, cingulate gyrus supporting retrieval processes⁶⁷, and insula integrating emotional components⁶⁶ - together enabling the formation of rich, contextual memories^{68,69}. Importantly, both super-MA and super-MS measures demonstrated predictive value for higher cognitive functions, including emotion regulation and fluid intelligence, establishing brain mediation networks as an effective framework for investigating

how indirect neural interactions support diverse cognitive processes. These findings collectively highlight the functional significance of mediated information transfer pathways in cognition, with distinct mediation patterns contributing differentially to self-regulatory and memory systems while both serving as reliable markers of cognitive information processing capacity.

The current study has several limitations that warrant consideration. First, although the cognitive prediction model based on brain super-mediation and mediated sets demonstrates statistical significance, the results are limited to resting-state data and underlying neural mechanisms need further validation. Subsequent investigations should incorporate task-based fMRI to systematically compare the similarities and differences in network characteristics between resting and task states, as well as their associations with cognitive functions. Second, while the linear mediation framework employed in the ICMN model aligns with current mainstream brain network analysis methods and offers computational efficiency advantages^{20,21,23,24}, it may not fully capture the nonlinear dynamic properties of the brain. Future work should focus on developing nonlinear mediation analysis algorithms that better reflect neurobiological characteristics⁷⁰⁻⁷². Finally, the current model only examines mediation relationships among three brain regions, without addressing more complex higher-order network interactions. Subsequent research should extend the analytical scope to multi-region systems and conduct systematic comparisons with advanced methods such as hypergraph models^{73,74} and partial correlation networks²⁹ to verify the robustness of the findings.

Methods

Data acquisition and preprocessing

The fMRI dataset used is from the Human Connectome Project (HCP)⁷⁵. We considered the 200 unrelated subjects as provided from the HCP 1200 subjects data release (108 females and 92 males, mean age = 29.2 ± 3.6 years). Human participants were recruited from Washington University (St. Louis, MO) and surrounding areas. All participants gave informed consent in accordance with policies approved by the University of Washington Institutional Review Board⁷⁶. All ethical regulations relevant to human research participants were followed. Participants in the HCP sample underwent various behavioral tests that were part of the NIH Toolbox battery, as well as several non-NIH Toolbox behavioral assessments. We primarily focused on 6 cognitive factors highlighted in the HCP data dictionary. The assessments of these cognitive factors include: self-regulation, episodic memory, vocabulary comprehension, emotion recognition, fluid cognition, and crystallized cognition.

The open-source HCP minimal preprocessing pipeline⁷⁷, version 3.5.0, was applied to all neuroimaging data. This included: anatomic reconstruction and segmentation; EPI reconstruction, segmentation, and spatial normalization to a standard template; intensity normalization; and motion correction. The resulting data were in CIFTI 64k-vertex grayordinate space, and all subsequent analyses were performed in MATLAB R2014b. Following minimal preprocessing, vertices were parcellated into 360 cortical regions per the atlas²⁵. To parcellate each of these regions, we calculated the average time series of enclosed vertices. According to Yeo's previous work, all regions were assigned to seven modules, namely Visual (Vis), Somatomotor (SM), Dorsal Attention (DA), Ventral Attention (VA), Frontoparietal (FP), Limbic (Lim), and Default mode (DM)⁷⁸.

We also used the CHCP dataset as a validation dataset. Details on data acquisition and preprocessing are provided in the Supplementary Methods.

Simulation computational modeling

We developed a large-scale neural network model comprising 400 brain regions organized into 8 functional modules (six non-hub and two hub modules) with specified intra-module (40–70%) and inter-

module (10–25%) connection probabilities weighted by Gaussian distributions. Neural dynamics were simulated using a standard neural mass model with hyperbolic tangent transfer functions⁷⁹, where node activity was governed by coupled differential equations with local and global coupling parameters set to unity and a time constant of 10 ms. Spontaneous activity was generated through Gaussian noise inputs (mean 0, SD 1), and the system was numerically integrated for 1200 s using a second-order Runge-Kutta method (10 ms time step). The resulting signals were convolved with a hemodynamic response function, standardized, and downsampled to 1-s temporal resolution to generate synthetic fMRI data for 30 virtual subjects (details are provided in Supplementary Methods).

ICMN modeling

The mediation analysis decomposes the total effect that an initial/independent variable (node X) has on a target/dependent variable (node Y) into an indirect effect that is transferred via a mediator (node M) and a conditional direct effect. Further, in addition to the three nodes above-mentioned, we considered the effects of other nodes in the brain on the mediation effect. We employed whole-brain time-series ICA results to replace the ICA results derived from the remaining brain nodes, based on the following rationale: First, calculating the mediation effects for any three brain regions while performing ICA separately on the remaining regions would impose an excessive computational burden. Second, systematic validation confirmed that the differences between the two approaches were negligible, both statistically and practically. We set 20 components (10 and 30 components as repeatability verification) for the whole brain. The single mediator model consists of three regression equations as follows:

$$Y_t = i_1 + \gamma_0 X_t + \delta_1 O_t + e_1 \quad (1)$$

$$M_t = i_2 + \alpha X_t + \delta_2 O_t + e_2 \quad (2)$$

$$Y_t = i_3 + \gamma X_t + \beta M_t + \delta_3 O_t + e_3 \quad (3)$$

where X_t is the time series of the initial variable (node X), M_t is the time series of the mediator (node M), Y_t is the time series of the target variable (node Y), O_t is the independent components of the time series in whole brain nodes, and e_1 , e_2 , e_3 are the residuals. In this model, γ_0 represents the total effect between node X and node Y , γ quantifies the direct effect from node X to Y , the product of α and β ($\alpha \cdot \beta$) quantifies the indirect effect of node X on Y through M , and δ_1 , δ_2 , δ_3 represent the whole brain effect in the mediation network model. The experiment required that statistical significance be tested in each of the three tests that comprise the path model (testing α , β and $\alpha \cdot \beta$), where the significance of the product of paths α and β was assessed by Sobel's test⁸⁰ to test for indirect effects. The standard process is as follows⁸¹:

(i) Sequential inspection coefficient α and β . If both are significant, proceed with step (ii), with at least one significant retest $\alpha \cdot \beta$. If not significant, the indirect effect does not exist, otherwise, execute step (ii);

(ii) Inspection coefficient γ . If significant, there is a partial mediating effect. If not significant, it represents complete mediation.

In the entire brain mediation network, the E_{xy}^m ($N \times N \times N$ connectivity matrices) was used to represent the entire mediation effects between node X , node Y , and node M , whose value range within the range of [0,1]. If it is partial mediation, the indirect effect is represented by calculating the proportion of the total effects to the indirect effects:

$$A_{M_t}(X_t, Y_t) = \frac{\alpha \beta}{\gamma_0} \quad (4)$$

If it is complete mediation, the value of the mediation effect is 1, while if there does not exist a mediation effect, the value is 0.

The brain mediation network metrics

AMM. AMM is calculated as follows:

$$AMM_{xy} = \frac{1}{N} \sum_{m=1}^N E_{xy}^m \quad (5)$$

where E_{xy}^m refers to the strength of the connection between node X and node Y mediated by node M . N represents the number of nodes in the whole brain.

MA. MA is defined as follows:

$$MA_m = \frac{1}{N \times N} \sum_{x=1, y=1}^{N, N} E_{xy}^m \quad (6)$$

Nodes with high mediation ability have higher information dissemination capability, which act as a bridge to other regions in their exchanges.

MS. MS is defined as follows:

$$MS_x = \frac{1}{2N} \sum_{y=1}^N (AMM_{xy} + AMM_{yx}) \quad (7)$$

where AMM_{xy} represents the size of the mediated information transfer from node X to node Y . Nodes with high MS indicate their information transmission with other regions passes through a third region more often than reaching directly.

The network analysis and cognition prediction

We used the Brain Connectivity Toolbox to calculate degree strength, global efficiency, and local efficiency of FC matrix. We also analyzed AMM and FC gradients using the BrainSpace toolbox⁸². The primary gradient, representing dominant cortical organization, was examined. We employed CPM⁸³ with leave-one-subject cross-validation. Super-MA/MS values and cognitive scores were used to train linear regression models on nodes showing significant Spearman correlations ($p < 0.05$). Predictive performance was evaluated by correlating predicted and actual cognitive scores. See Supplementary Methods for more details.

Statistics and reproducibility

The simulation experiment included 30 participants, while the real fMRI experiment involved 200 participants. For brain regional analyses, we utilized averaged subject data derived from 400-region and 360-region brain parcellations, respectively. A one-sample t -test tested the significance of module MA/MS relative to the mean. The relationship between MA/MS and topological properties was evaluated using linear and quadratic regression models. The Akaike information criterion (AIC) compared the fit of these models. Spearman correlation was employed to assess correlations between FC and AMM, and their gradient correlations. All statistical tests involving module analysis were corrected for multiple comparisons using the Bonferroni method. The relationship between super-MAs/super-MSs and cognitive performance is also through Spearman correlation. Gender, age, and years were considered irrelevant variables and were regressed out. A significance threshold of $p < 0.05$ was applied to all tests, to determine statistical relevance. This study employed a cross-sectional design without repeated experiments or measurements.

Data availability

The MRI dataset used in this paper is available in the Human Connectome Project (<https://www.humanconnectome.org>) and the CHCP (<https://doi.org/10.11922/sciencedb.01374>). The source data used for generating Figs. 2–9 are provided in Supplementary Data 1.

Code availability

The codes used in this paper are available on GitHub (https://github.com/WANG-BIN-LAB/Brain_Mediation_Network).

References

1. Lynn, C. W. & Bassett, D. S. The physics of brain network structure, function and control. *Nat. Rev. Phys.* **1**, 318–332 (2019).
2. Wandell, B. A., Dumoulin, S. O. & Brewer, A. A. Visual field maps in human cortex. *Neuron* **56**, 366–383 (2007).
3. Daskalakis, Z. J. et al. Exploring the connectivity between the cerebellum and motor cortex in humans. *J. Physiol.* **557**, 689–700 (2004).
4. Edde, M., Leroux, G., Altena, E. & Chanraud, S. Functional brain connectivity changes across the human life span: from fetal development to old age. *J. Neurosci. Res.* **99**, 236–262 (2021).
5. Mercado III, E. Neural and cognitive plasticity: from maps to minds. *Psychol. Bull.* **134**, 109–137 (2008).
6. Ogawa, S., Lee, T. M., Kay, A. R. & Tank, D. W. Brain magnetic resonance imaging with contrast dependent on blood oxygenation. *Proc. Natl Acad. Sci. USA* **87**, 9868–9872 (1990).
7. Zalesky, A., Fornito, A. & Bullmore, E. On the use of correlation as a measure of network connectivity. *Neuroimage* **60**, 2096–2106 (2012).
8. Yaesoubi, M., Allen, E. A., Miller, R. L. & Calhoun, V. D. Dynamic coherence analysis of resting fMRI data to jointly capture state-based phase, frequency, and time-domain information. *Neuroimage* **120**, 133–142 (2015).
9. Friston, K., Moran, R. & Seth, A. K. Analysing connectivity with Granger causality and dynamic causal modelling. *Curr. Opin. Neurobiol.* **23**, 172–178 (2013).
10. Park, C.-H., Lee, S., Kim, T., Won, W. Y. & Lee, K.-U. Different alterations in brain functional networks according to direct and indirect topological connections in patients with schizophrenia. *Schizophr. Res.* **188**, 82–88 (2017).
11. Parsons, N. et al. Structural-functional connectivity bandwidth of the human brain. *Neuroimage* **263**, 119659 (2022).
12. Ward, A. M. et al. The parahippocampal gyrus links the default-mode cortical network with the medial temporal lobe memory system. *Hum. Brain Mapp.* **35**, 1061–1073 (2014).
13. Das, P. et al. Pathways for fear perception: modulation of amygdala activity by thalamo-cortical systems. *Neuroimage* **26**, 141–148 (2005).
14. Battiston, F. et al. The physics of higher-order interactions in complex systems. *Nat. Phys.* **17**, 1093–1098 (2021).
15. Petrican, R., Fornito, A., Murgatroyd, C., Boyland, E. & Hardman, C. A. Genetic risk predicts adolescent mood pathology via sexual differentiation of brain function and physiological aging. *Nat. Commun.* **16**, 5593 (2025).
16. Lucas, M., Wagshul, M., Izzetoglu, M. & Holtzer, R. Moderating effect of white matter integrity on brain activation during dual-task walking in older adults. *J. Gerontol. Ser. A* **74**, 435–441 (2018).
17. Kim, Y.-K., Ham, B.-J. & Han, K.-M. Interactive effects of genetic polymorphisms and childhood adversity on brain morphologic changes in depression. *Prog. Neuropsychopharmacol. Biol. Psychiatry* **91**, 4–13 (2019).
18. Ao, Y., Klar, P., Catal, Y., Wang, Y. & Northoff, G. Infra-slow scale-free dynamics modulate the connection of neural and behavioral variability during attention. *Commun. Biol.* **8**, 1057 (2025).
19. Imai, K., Keele, L. & Yamamoto, T. Identification, inference and sensitivity analysis for causal mediation effects. *Stat. Sci.* **25**, 51–71 (2010).
20. Kaboodvand, N., Bäckman, L., Nyberg, L. & Salami, A. The retrosplenial cortex: a memory gateway between the cortical default mode network and the medial temporal lobe. *Hum. Brain Mapp.* **39**, 2020–2034 (2018).
21. Zhao, Y. & Luo, X. Granger mediation analysis of multiple time series with an application to functional magnetic resonance imaging. *Biometrics* **75**, 788–798 (2019).
22. Hu, K. Investigations into ventral prefrontal cortex using mediation models. *J. Neurosci. Res.* **98**, 632–642 (2020).
23. Kim, H.-C. et al. Mediation analysis of triple networks revealed functional feature of mindfulness from real-time fMRI neurofeedback. *Neuroimage* **195**, 409–432 (2019).
24. Chén, O. Y. et al. Identifying neural signatures mediating behavioral symptoms and psychosis onset: High-dimensional whole brain functional mediation analysis. *Neuroimage* **226**, 117508 (2021).
25. Glasser, M. F. et al. A multi-modal parcellation of human cerebral cortex. *Nature* **536**, 171–178 (2016).
26. Schaefer, A. et al. Local-global parcellation of the human cerebral cortex from intrinsic functional connectivity MRI. *Cereb. Cortex* **28**, 3095–3114 (2018).
27. Santoro, A., Battiston, F., Lucas, M., Petri, G. & Amico, E. Higher-order connectomics of human brain function reveals local topological signatures of task decoding, individual identification, and behavior. *Nat. Commun.* **15**, 10244 (2024).
28. Varley, T. F., Pope, M., Faskowitz, J. & Sporns, O. Multivariate information theory uncovers synergistic subsystems of the human cerebral cortex. *Commun. Biol.* **6**, 1–12 (2023).
29. Makhtar, S. N., Senik, M. H., Stevenson, C. W., Mason, R. & Halliday, D. M. Improved functional connectivity network estimation for brain networks using multivariate partial coherence. *J. Neural Eng.* **17**, 026013 (2020).
30. Seguin, C., Sporns, O. & Zalesky, A. Brain network communication: concepts, models and applications. *Nat. Rev. Neurosci.* **24**, 557–574 (2023).
31. Heuvel, M. P. vanden & Sporns, O. Network hubs in the human brain. *Trends Cogn. Sci.* **17**, 683–696 (2013).
32. Zhou, D. et al. Efficient coding in the economics of human brain connectomics. *Netw. Neurosci.* **6**, 234–274 (2022).
33. Estrada, E., Higham, D. J. & Hatano, N. Communicability betweenness in complex networks. *Phys. Stat. Mech. Its Appl.* **388**, 764–774 (2009).
34. Wang, J. et al. Parcellation-dependent small-world brain functional networks: a resting-state fMRI study. *Hum. Brain Mapp.* **30**, 1511–1523 (2009).
35. Bullmore, E. & Sporns, O. The economy of brain network organization. *Nat. Rev. Neurosci.* **13**, 336–349 (2012).
36. Rubinov, M. & Sporns, O. Complex network measures of brain connectivity: uses and interpretations. *Neuroimage* **52**, 1059–1069 (2010).
37. Sepulcre, J. et al. The organization of local and distant functional connectivity in the human brain. *PLOS Comput. Biol.* **6**, e1000808 (2010).
38. Tong, C. et al. Multimodal analysis demonstrating the shaping of functional gradients in the marmoset brain. *Nat. Commun.* **13**, 6584 (2022).
39. Nenning, K.-H. et al. Omnipresence of the sensorimotor-association axis topography in the human connectome. *Neuroimage* **272**, 120059 (2023).
40. Huntenburg, J. M., Bazin, P.-L. & Margulies, D. S. Large-scale gradients in human cortical organization. *Trends Cogn. Sci.* **22**, 21–31 (2018).

41. Margulies, D. S. et al. Situating the default-mode network along a principal gradient of macroscale cortical organization. *Proc. Natl. Acad. Sci. USA* **113**, 12574–12579 (2016).

42. Wang, X. et al. The Brain's topographical organization shapes dynamic interaction patterns that support flexible behavior based on rules and long-term knowledge. *J. Neurosci.* **44**, e2223232024 (2024).

43. Xia, M. et al. Shared and Distinct Functional Architectures of Brain Networks Across Psychiatric Disorders. *Schizophr. Bull.* **45**, 450 (2018).

44. Taguchi, T., Kitazono, J., Sasai, S. & Oizumi, M. Association of bidirectional network cores in the brain with conscious perception and cognition. *bioRxiv* 2024.04.30.591001 <https://doi.org/10.1101/2024.04.30.591001> (2024).

45. Luppi, A. I. et al. A synergistic core for human brain evolution and cognition. *Nat. Neurosci.* **25**, 771–782 (2022).

46. Corbetta, M. & Shulman, G. L. Control of goal-directed and stimulus-driven attention in the brain. *Nat. Rev. Neurosci.* **3**, 201–215 (2002).

47. Hopfinger, J. B., Buonocore, M. H. & Mangun, G. R. The neural mechanisms of top-down attentional control. *Nat. Neurosci.* **3**, 284–291 (2000).

48. Rajan, A. et al. The microstructure of attentional control in the dorsal attention network. *J. Cogn. Neurosci.* **33**, 965–983 (2021).

49. Raccah, O., Daitch, A. L., Kucyi, A. & Parvizi, J. Direct cortical recordings suggest temporal order of task-evoked responses in human dorsal attention and default networks. *J. Neurosci.* **38**, 10305–10313 (2018).

50. Macaluso, E. Orienting of spatial attention and the interplay between the senses. *Cortex* **46**, 282–297 (2010).

51. Cieslik, E. C., Zilles, K., Grefkes, C. & Eickhoff, S. B. Dynamic interactions in the fronto-parietal network during a manual stimulus-response compatibility task. *Neuroimage* **58**, 860–869 (2011).

52. Kang, Y. et al. Identifying influential nodes in brain networks via self-supervised graph-transformer. *Comput. Biol. Med.* **186**, 109629 (2025).

53. Ioannides, A. A. et al. Spatiotemporal profiles of visual processing with and without primary visual cortex. *Neuroimage* **63**, 1464–1477 (2012).

54. Troncoso, X. G., Macknik, S. L. & Martinez-Conde, S. Vision's first steps: anatomy, physiology, and perception in the retina, lateral geniculate nucleus, and early visual cortical areas. In *Visual Prosthetics: Physiology, Bioengineering, Rehabilitation* (ed. Dagnelie, G.) 23–57 (Springer US, Boston, 2011); https://doi.org/10.1007/978-1-4419-0754-7_2.

55. Bi, Y., Wang, X. & Caramazza, A. Object domain and modality in the ventral visual pathway. *Trends Cogn. Sci.* **20**, 282–290 (2016).

56. Qin, W. & Yu, C. Neural pathways conveying nonvisual information to the visual cortex. *Neural Plast.* **2013**, 864920 (2013).

57. Henderson, M. M., Serences, J. T. & Rungratsameetaweemana, N. Dynamic categorization rules alter representations in human visual cortex. *Nat. Commun.* **16**, 3459 (2025).

58. Namkung, H., Kim, S.-H. & Sawa, A. The insula: an underestimated brain area in clinical neuroscience, psychiatry, and neurology. *Trends Neurosci.* **40**, 200–207 (2017).

59. Kimura, Y. et al. An anatomo-functional study of the interactivity between the paracentral lobule and the primary motor cortex. *J. Neurosurg.* **141**, 1096–1104 (2024).

60. Beauchamp, M. S. See me, hear me, touch me: multisensory integration in lateral occipital-temporal cortex. *Curr. Opin. Neurobiol.* **15**, 145–153 (2005).

61. Haxby, J. V., Hoffman, E. A. & Gobbini, M. I. The distributed human neural system for face perception. *Trends Cogn. Sci.* **4**, 223–233 (2000).

62. Shenhar, A., Botvinick, M. M. & Cohen, J. D. The expected value of control: an integrative theory of anterior cingulate cortex function. *Neuron* **79**, 217–240 (2013).

63. Sitaram, R. et al. Mechanisms of brain self-regulation: psychological factors, mechanistic models and neural substrates. *Philos. Trans. R. Soc. Lond. B. Biol. Sci.* **379**, 20230093 (2024).

64. Kim, S., Dalbó da Rocha, J. L., Birbaumer, N. & Sitaram, R. Self-Regulation of the posterior-frontal brain activity with real-time fMRI neurofeedback to influence perceptual discrimination. *Brain Sci.* **14**, 713 (2024).

65. Langner, R., Leiberg, S., Hoffstaedter, F. & Eickhoff, S. B. Towards a human self-regulation system: Common and distinct neural signatures of emotional and behavioural control. *Neurosci. Biobehav. Rev.* **90**, 400–410 (2018).

66. Rolls, E. T. The cingulate cortex and limbic systems for emotion, action, and memory. *Brain Struct. Funct.* **224**, 3001–3018 (2019).

67. Gasquoine, P. G. Contributions of the insula to cognition and emotion. *Neuropsychol. Rev.* **24**, 77–87 (2014).

68. Westphal, A. J., Wang, S. & Rissman, J. Episodic memory retrieval benefits from a less modular brain network organization. *J. Neurosci.* **37**, 3523–3531 (2017).

69. He, X. et al. Multi-level cognitive state classification of learners using complex brain networks and interpretable machine learning. *Cogn. Neurodyn.* **19**, 5 (2025).

70. Motlaghian, S. M. et al. A method for estimating and characterizing explicitly nonlinear dynamic functional network connectivity in resting-state fMRI data. *J. Neurosci. Methods* **389**, 109794 (2023).

71. Jeong, S.-O. et al. Empirical Bayes estimation of pairwise maximum entropy model for nonlinear brain state dynamics. *Neuroimage* **244**, 118618 (2021).

72. Chen, Y., Liu, Z.-W. & Qin, Y. Finite-time topology identification of delayed complex dynamical networks and its application. *Cyborg Bionic Syst. Wash. DC* **5**, 0092 (2024).

73. Xiao, L. et al. Multi-Hypergraph Learning-Based Brain Functional Connectivity Analysis in fMRI Data. *IEEE Trans. Med. Imaging* **39**, 1746–1758 (2020).

74. Song, X., Wu, K. & Chai, L. Brain Network analysis of schizophrenia patients based on hypergraph signal processing. *IEEE Trans. Image Process.* **32**, 4964–4976 (2023).

75. Van Essen, D. C. et al. The WU-Minn Human Connectome Project: an overview. *Neuroimage* **80**, 62–79 (2013).

76. Smith, S. M. et al. Functional connectomics from resting-state fMRI. *Trends Cogn. Sci.* **17**, 666–682 (2013).

77. Glasser, M. F. et al. The minimal preprocessing pipelines for the Human Connectome Project. *Neuroimage* **80**, 105–124 (2013).

78. Yeo, B. T. T. et al. The organization of the human cerebral cortex estimated by intrinsic functional connectivity. *J. Neurophysiol.* **106**, 1125–1165 (2011).

79. Cole, M. W., Ito, T., Bassett, D. S. & Schultz, D. H. Activity flow over resting-state networks shapes cognitive task activations. *Nat. Neurosci.* **19**, 1718–1726 (2016).

80. Sobel, M. E. Asymptotic confidence intervals for indirect effects in structural equation models. *Sociol. Methodol.* **13**, 290–312 (1982).

81. Wen, Z. L. & Ye, B. J. Analyses of mediating effects: the development of methods and models. *Adv. Psychol. Ence* **22**, 731–745 (2014).

82. Vos de Wael, R. et al. BrainSpace: a toolbox for the analysis of macroscale gradients in neuroimaging and connectomics datasets. *Commun. Biol.* **3**, 103 (2020).

83. Shen, X. et al. Using connectome-based predictive modeling to predict individual behavior from brain connectivity. *Nat. Protoc.* **12**, 506–518 (2017).

Acknowledgements

This work was supported by the National Natural Science Foundation of China (grant numbers 62406025, 62576240, 62176177, 62336002); the Key-Area Research and Development Program of Guangdong Province (grant number 2023B0303030002); the STI 2030-Major Projects (grant number 2022ZD0208500); the Beijing Nova program (grant number

20230484465); and the Science and Technology Cooperation and Exchange Special Projects of Shanxi (grant number 202304041101034).

Author contributions

B.W. conceptualized the study. X.Z. performed the numerical analysis and wrote the original draft of the manuscript. T.P. developed the code and prepared the figures. T. Li completed the overall replication of results. T. Liu reviewed and supervised the manuscript. T.Y. provided funding support. All authors contributed to the review and editing of the draft.

Competing interests

The authors declare no competing interests.

Additional information

Supplementary information The online version contains supplementary material available at <https://doi.org/10.1038/s42003-025-08948-2>.

Correspondence and requests for materials should be addressed to Tiantian Liu or Tianyi Yan.

Peer review information *Communications Biology* thanks Fabrizio Parente, Andrea Brovelli, and the other, anonymous, reviewer(s) for their contribution to the peer review of this work. Primary Handling Editor: Jasmine Pan. A peer review file is available.

Reprints and permissions information is available at <http://www.nature.com/reprints>

Publisher's note Springer Nature remains neutral with regard to jurisdictional claims in published maps and institutional affiliations.

Open Access This article is licensed under a Creative Commons Attribution-NonCommercial-NoDerivatives 4.0 International License, which permits any non-commercial use, sharing, distribution and reproduction in any medium or format, as long as you give appropriate credit to the original author(s) and the source, provide a link to the Creative Commons licence, and indicate if you modified the licensed material. You do not have permission under this licence to share adapted material derived from this article or parts of it. The images or other third party material in this article are included in the article's Creative Commons licence, unless indicated otherwise in a credit line to the material. If material is not included in the article's Creative Commons licence and your intended use is not permitted by statutory regulation or exceeds the permitted use, you will need to obtain permission directly from the copyright holder. To view a copy of this licence, visit <http://creativecommons.org/licenses/by-nc-nd/4.0/>.

© The Author(s) 2025